International Journal of Engineering & Technology, 7 (4.39) (2018) 65-73

International Journal of Engineering & Technology

Website: www.sciencepubco.com/index.php/IJET

Research paper

A Multicopter Ground Testbed for the Evaluation of Attitude and Position Controller

Nguyen Xuan-Mung[1], Sung-Kyung Hong[2]*

[1 2]Faculty of Mechanical and Aerospace Engineering, Sejong University, Seoul, South Korea
**Corresponding author E-mail: skhong@sejong.ac.kr*

Abstract

A ground testbed system to evaluate the performance of attitude and position control of multicopters is proposed in this paper. The system consists of a vehicle attached to a base via a sphere joint which allows the vehicle to rotate about the three axes roll, pitch and yaw. In addition, a pseudo positioning algorithm is presented to simulate the position of the vehicle based on a force sensor and an inertial measurement unit sensor. A global positioning system simulator is used to provide the artificial GPS signal based on the simulated position signal during the indoor trials. The proposed system provides the multicopters with all six degrees of freedom during flight allowing the vehicle to perform as if it were in actual flight. Several experimental flight tests are conducted to prove the effectiveness of the proposed system.

Keywords: *Ground testbed, test bench, hardware-in-the-loop simulation, multicopter, quadrotor, 6-DOF flight.*

1. Introduction

In recent years, unmanned aerial vehicles (UAVs) have become increasingly popular with the researches of aerial robotics due to their many advantages such as high maneuverability, diverse applicability, reliability, and economy. Technological advanced have allowed the UAVs to become smaller and lighter. Multicopters, also referred to as multirotor, are the most popular type of UAV and have attracted worldwide attention. Due to their simple structure, they are easily designed and manufactured at an affordable cost. Moreover, due to the ready availability of mathematical models and the multicopters' exceptional agility, they can be controlled to perform a variety of complex tasks. These factors have contributed to their popularity and ubiquity in a broad range of applications that includes scientific research, civil engineering, military applications, aerial mapping, search and rescue operations, and risk zone inspection, etc. [1-4].

Developing a multicopter vehicle is time consuming and complicated. The typical development process of a multicopter usually consists of several phases: system design, modelling, controller design, simulation, and real flight tests [1-3]. Generally, there is a considerable difference between the controller's performance during a simulation and a real flight. Therefore, the flight test usually faces several critical failures and experiences a long period [4]. Furthermore, the actual test is usually costly and risky. Meanwhile, a ground testbed (GTB) allows multicopter developers to repeatedly tune their controllers and test the control performance in a quick and reliable manner. On the GTB, vehicles can perform flights without crashing, endangering people, or damaging the surroundings.

Several GTB systems have been developed. An approach is presented in [3] for a 2-DOF hardware-in-the-loop (HIL) testbed for testing longitudinal, lateral, and heading control of small helicopters (Figure 1c). This testbed consists of a long pole, anchored to the ground, and a headpiece connected to the pole through a mechanical structure. The testbed uses a mathematical model of the helicopter to simulate motion and calculate state information of the vehicle. Although the testbed allows for testing and tuning of the controller in both hover and trajectory mode, it cannot perform the longitudinal and lateral controls simultaneously due to a lacking DOF. Another approach presented in [5] introduces a testbed for quadcopter attitude stabilization control (Figure 1a). This three Degree of Freedom (DOF) testbed is small, simple but affordable. By using a single pole with a sphere joint, the testbed allows the quadcopter to rotate about the three Euler angles but not to perform a position flight. In a recent study [6], the authors proposed a 3-DOF test bench which consists of a support and a rotation joint. The test bench is useful to identify model parameters and test attitude controllers of quadcopter. However, due to a lacking DOF this system cannot be used to test the quadcopter's position controller.

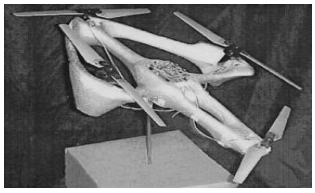

(a)

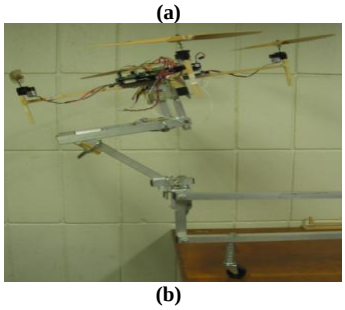

(b)

(c)

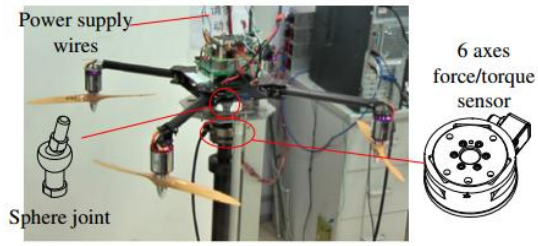

(d)

Figure 1: Some GTBs presented in the literature

In [7], the authors described a 5-DOF testbed, called Whiteman training stand, for a small quadcopter (Figure 1b). The testbed allows the quadcopter to hover as the quadcopter is able to rotate about its three Euler angles. The arm of the stand also allows the quadcopter perform altitude flight. However, position control cannot be performed as the training stand has no positioning unit. Yet another approach involving a 6-DOF test bench (Figure 1d) is described in [2], where the test bench consists of a stand, a 6-axes force/torque sensor, a sphere joint, and a quadcopter. The quadcopter is equipped with an inertial measurement unit (IMU) and a digital signal processor (DSP) to process input and output data. The test bench is capable to perform a 6-DOF flight in position hold mode but unable to perform a target position approach flight because of the structure's vibration and sensor noise [2]. Besides that, this test bench may not be suitable for other quadcopter platforms that are equipped with flight control units (FCU) that differ from the DSP used in [2] because of incompatibilities in communication protocols between the devices. The references [2-12] indicate performing position flights on a GTB is a challenge for multicopter researchers. Most of the previous GTBs are only capable of 2-DOF, 3-DOF, or 5-DOF flights with only very few capable of providing the full 6-DOF capabilities. Current GTBs still need to be improved in order to meet the higher requirements posed by real-world applications. In this study, we propose a 6-DOF GTB for multicopters. With a stand that is firmly fixed on the ground, the GTB is suitable for both small and large force and torque simulations. A force sensor is utilized to measure vehicle thrust. A pseudo positioning algorithm simulates translational positions of the vehicle based on the measured thrust and the IMU data. A global positioning system (GPS) simulator emits the simulated position information in the indoor environment allowing any multicopter which equipped with a standard GPS receiver to receive the position feedback. The main contribution of this paper is twofold: 1) the proposed GTB allows multicopters to perform 6-DOF flight as if it were in actual flight. This indicates that multicopter developers can use the GTB to preliminarily verify and refine new 6-DOF control algorithms though indoor trials before applying them to the real system, which could significantly reduce the experimental risks and costs; and 2) the GTB is applicable for various types of flight platform which equipped with different types of FCU and sensor. Several flights on the GTB, i.e., attitude stabilized, altitude, and position flights, were conducted to verify the value of the system.

The rest parts of this paper are organized as follows: Section 2 describes the system hardware and software structure. Section 3 presents the pseudo positioning algorithm. The dynamics model and controller of quadcopter are described in section 4. Section 5 presents the experimental results followed by conclusions.

2. System Structure

2.1. Hardware

The GTB consists of a base, a vehicle, and a control station (see Figure 2a). The base is a large stand with one end firmly fixed on the ground and the other end equipped with a force sensor. The vehicle used in this study is a quadcopter, at its base attached to the stand through a spherical joint. This joint transmits the forces acting upon the vehicle to the force sensor and allows the vehicle to rotate about the three Euler angles. Since the joint is small and lightweight, the mass and friction can be ignored in the analyses.

The quadcopter is equipped with aviation electronic and a Pixhawk flight computer unit (FCU) which includes an inertial measurement unit (IMU) to provide information about the vehicle's attitude and angular rate. The vehicle receives simulated GPS signals. The control station consists of a personal computer (PC), a GPS simulator, and an RC transmitter. The thrust force is measured via a commercially available data acquisition (DAQ) box.

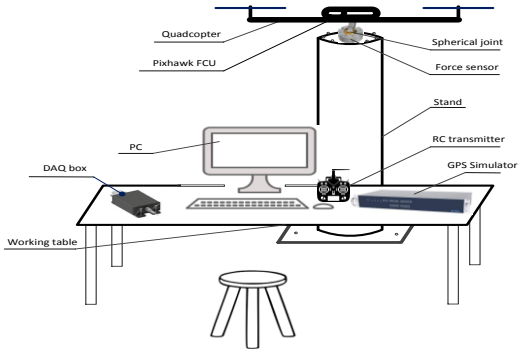

a) Hardware

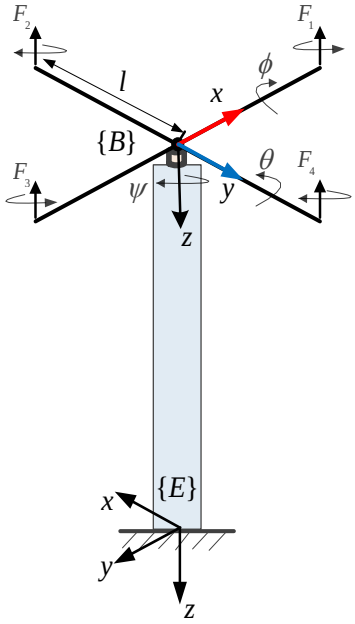

b) Coordinate systems

Figure 2: The ground testbed scheme

2.2. Software

Definition 1 (pseudo positioning algorithm): A pseudo positioning algorithm (PPA) is an algorithm which simulates translational positions of a non-moving vehicle mounted to a GTB from the force sensor's measurements and IMU sensor's data.

Definition 2 (pseudo position): The position provided by the PPA is called pseudo position.

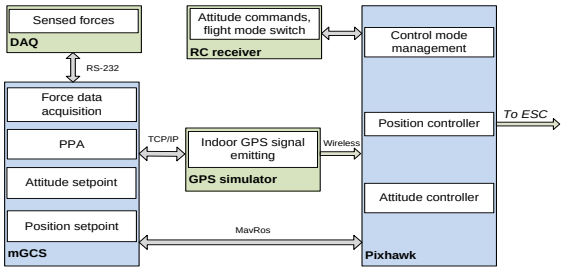

Figure 3: The software structure

A program called mGCS has been built to serve as a control station program which provides the following functions:
- Func. 1: User's command of attitude and position.
- Func. 2: Vehicle's attitude and angular rate acquisition.
- Func. 3: Thrust force acquisition.
- Func. 4: PPA operation.
- Func. 5: Vehicle's pseudo position broadcasting and visualization.

For Functions 1 and 2, mGCS connects to the FCU using wireless MavRos [13] [14] protocol at a frequency of 50 Hz. Using these functions, users can manually send either attitude or position commands to the vehicle. Simultaneously, mGCS receives IMU sensor's feedback data, and use them for calculating in the PPA. For Function 3, mGCS is connected to the DAQ box via serial protocol on RS-232 port at a baud rate of 115200 bps. A low pass filter (LPF) is applied to reduce noise in the thrust data. Functions 4 operates the PPA at 100 Hz to simulate the vehicle's pseudo positions. Function 5 operates at 10 Hz to send the pseudo positions to the GPS simulator via TCP/IP protocol and display the pseudo positions on a visualization window of mGCS.
The GPS simulator is operated by its particular driver and receives the pseudo positions from mGCS, processes them, and emits indoor artificial GPS signals. The FCU contains an attitude and a position controller which utilize the IMU's data and the received indoor GPS signals. The whole software structure and communication protocols are described in Figure 3.

3. Pseudo Positioning Algorithm

Through analyzing a quadcopter dynamics along *x*-direction, a comparison between traditional algorithm and modified algorithm is presented in subsections 3.2 and 3.3 to highlight the soundness of the proposed method. Afterward, subsection 3.4 presents a procedure to obtain the parameters of the modified algorithm. The approaches for the PPA along *y*-direction and *z*-direction, respectively, can be analyzed by performing some similar steps as given in this section which are omitted for brevity.

3.1. Coordinate Systems

Figure 2b presents coordinate systems to be used in this study. In the body frame {*B*}, the origin is at the center of gravity of the vehicle, the *x* axis points out the nose, the *y* axis points out the right side of the vehicle, and the *z* axis points toward the belly [15,16]. The body frame is the reference used for estimating the attitude, angular rates of the vehicle, and also for attitude controller design.

In the north-east-down (NED) inertial frame {*E*}, the origin is usually located at the position the base is fixed on the ground, the *x* axis points North, the *y* axis points East, and the *z* axis points downward the center of the earth. The inertial frame is used for the PPA and for the position controller design.

Denote the three Euler angles roll, pitch, and yaw by f, θ, and ψ, respectively. Where, $|f| < \pi/2$, $|\theta| < \pi/2$, and $|\psi| \le \pi$. The rotation matrix representing the orientation of {*B*} with respect to {*E*} is as the following [17]:

$$R_B^E = \begin{pmatrix} c\theta c\psi & sf s\theta c\psi - cf s\psi & cf s\theta c\psi + sf s\psi \\ c\theta s\psi & sf s\theta s\psi + cf c\psi & cf s\theta s\psi - sf c\psi \\ -s\theta & sf c\theta & cf c\theta \end{pmatrix} \quad (1)$$

where, $ci \square \cos i$ and $si \square \sin i$ ($i = f, \theta, \psi$).

3.2. Traditional Algorithm

The traditional algorithm is based on typical quadcopter models in the body frame {*B*} with an assumption that only gravity (*mg*) and thrust force (*T*) are the forces acting significantly on the vehicle body, while other forces are negligible [17-18]:

$$\begin{cases} \dot{u} = -g\sin\theta + rv - qw \\ \dot{v} = g\sin f\cos\theta + pw - ru \\ \dot{w} = g\cos f\cos\theta + qu - pv - T/m \end{cases} \quad (2)$$

where *u*, *v*, and *w* represent the velocities in the *x*, *y*, and *z* directions, respectively, *p*, *q*, and *r* are the angular velocities of the vehicle corresponding to the *x*, *y*, and *z* axes, respectively.
Taking a look at the *x*-direction term, the first equation in expression (2), it can be seen that if the quadcopter tilts a small constant pitch angle of θ_c then the acceleration along to the *x* axis can be approximately calculated as:

$$\dot{u} = -g\theta_c \quad (3)$$

Integration of (3) yields:

$$u = -g\theta_c t + u_0 \quad (4)$$

Expression (4) implies that the velocity *u* tends toward infinity as the time *t* becomes infinite (see Figure 4a). However, in actual flight, even the quadcopter keeps tilting a constant pitch angle as time goes, its velocity cannot exceed a specific maximum. This inherent contradiction demonstrates the main weakness of the traditional model which is simply unsuitable for calculating both velocity and position of the vehicle. To overcome this shortcoming of the traditional algorithm, a modified algorithm is presented in the following subsection.

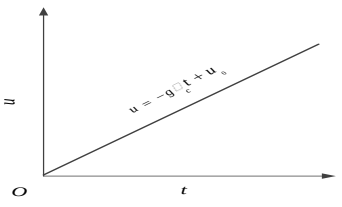

(a)

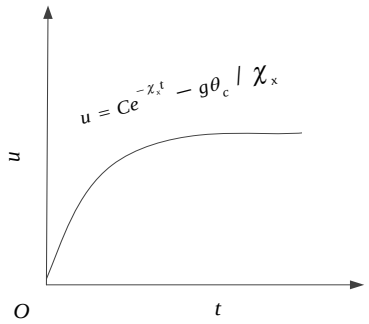

(b)

Figure 4: Traditional estimated velocity and innovated estimated velocity

3.3. Modified Algorithm

An alternative model has been proposed in [19-22] based on the assumption that beside of the gravity and thrust force, there is another term, call drag force, which needs to be considered. The model is as follows:

$$\begin{cases} \dot{u} = -g\sin\theta + rv - qw - \chi_x u \\ \dot{v} = g\sin f\cos\theta + pw - ru - \chi_y v \\ \dot{w} = g\cos f\cos\theta + qu - pv - T/m - \chi_z w \end{cases} \quad (5)$$

where, χ_x and χ_y are the drag force coefficients corresponding to the x and y axes, respectively. χ_x and χ_y can depend on several factors, but for nominal autonomous flight conditions they can be treated as constants [19].
After linearization at hover position, expression (5) can be rewritten as the followings:

$$\begin{cases} \dot{u} = -\chi_x u - g\theta \\ \dot{v} = -\chi_y v + gf \\ \dot{w} = -\chi_z w + g - T/m \end{cases} \quad (6)$$

Solving the first equations in expression (6) for a constant value θ_c of the pitch angle, we obtain:

$$u = C_1 e^{-\chi_x t} - g\theta_c / \chi_x \quad (7)$$

where, C_1 is a constant. Figure 4b shows the forward velocity u with respect to time. It is seen that with a constant tilting angle the velocity converges to a specific value. This confirms that the modified model is suitable for estimating the velocity and position of the vehicle.
To apply this modified algorithm to the PPA, the drag coefficients are obtained through a method presented in subsection 3.4. Figure 5 shows the block diagram of the proposed PPA which employs expression (6) to calculate the pseudo translational acceleration, velocity, and position of the vehicle.

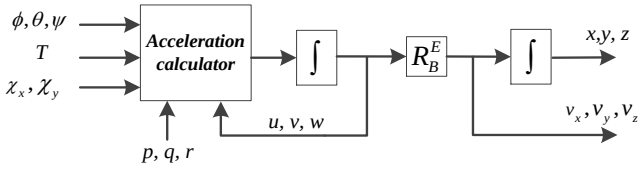

Figure 5: The PPA's block diagram

The simulated velocity v_x, v_y, and v_z in the inertial frame can be obtained as follows:

$$\begin{pmatrix} v_x \\ v_y \\ v_z \end{pmatrix}_{\{E\}} = R_B^E \begin{pmatrix} u \\ v \\ w \end{pmatrix}_{\{B\}} \quad (8)$$

where p_n, p_e, and h represent positions of the vehicle in the x, y, and z directions, respectively.

3.4. Drag Coefficient Estimation

Several studies have introduced methods to obtain the drag force coefficient [19] [20]. This subsection briefly presents a procedure to the obtain drag coefficients that best describe the drag force acting on the flight platform using in this study. Actual flights were conducted to get data for the analysis. To obtain the coefficients, we need the translational acceleration, velocity, and the attitude of the vehicle. The accelerations $a_x$is measured by the IMU sensor. An LPF with a cut-off frequency of 3Hz is applied to the acceleration data to eliminate sensor noise. The vehicle's velocities in the inertial frame $\{E\}$ are provided by a commercial GPS receiver are used as reliable references. These velocities are transformed into the body-frame velocities before for use in the subsequent analyses.
On one hand, the drag coefficient is considered to be proportional to the velocity as the followings [19] [20]:

$$u \approx -a_x / \chi_x \quad (9)$$

The drag coefficients χ_x that best satisfies the equation (9) are obtained through trial-and-error (Figure 6a).
On the other hand, this coefficient satisfies the equation (6).

$$\dot{u}_\theta = -\chi_x u_\theta - g\theta \quad (10)$$

The velocity u_θ, called estimated velocity, are calculated from the drag coefficient and the attitude. This estimated velocity is compared to the corresponding measured velocities to test the reliability of the obtained coefficients (Figure 6b).

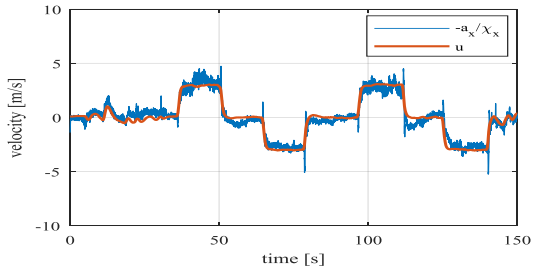

(a)

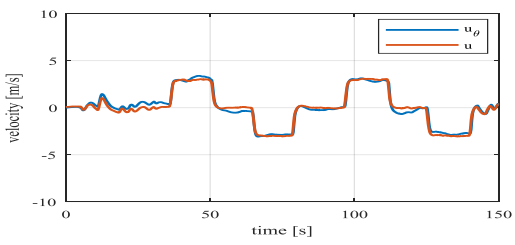

(b)

Figure 6: Comparison between $-a_x / \chi_x$, u_θ, and u

4. Quadcopter Dynamics Modelling and Control Design

In many previous studies, the modeling and control of quadcopter have been clearly proposed and verified through simulations and experiments [23-26]. In this section, the dynamics model and control of the quadcopter used in the experimental tests are briefly presented.

4.1. Quadcopter Dynamics Model

Let J_x, J_y, and J_z denote the moments of inertia of the quadcopter along x, y, and z axis, respectively, m represents the mass of vehicle; l denotes the arm length of vehicle, and g denotes the gravitational acceleration. The quadcopter's dynamics model is described as follows [23] [25]:

$$\begin{cases} \ddot{f} = \left(\dfrac{J_y - J_z}{J_x}\right)\dot{\theta}\dot{\psi} + \dfrac{l}{J_x}U_2 \\ \ddot{\theta} = \left(\dfrac{J_z - J_x}{J_y}\right)\dot{f}\dot{\psi} + \dfrac{l}{J_y}U_3 \\ \ddot{\psi} = \left(\dfrac{J_x - J_y}{J_z}\right)\dot{f}\dot{\theta} + \dfrac{1}{J_z}U_4 \\ \ddot{x} = \dfrac{1}{m}\left(\cos f \sin\theta\cos\psi + \sin f \sin\psi\right)U_1 \\ \ddot{y} = \dfrac{1}{m}\left(\cos f \sin\theta\sin\psi - \sin f \cos\psi\right)U_1 \\ \ddot{z} = g - \dfrac{1}{m}\left(\cos f \cos\theta\right)U_1 \end{cases} \tag{11}$$

where, U_i (i= 1, 2, 3, 4) denote the control inputs which are described as [2] [23]:

$$\begin{cases} U_1 = F_1 + F_3 + F_2 + F_4 \\ U_2 = F_4 - F_2 + mgd_J \cos\theta \sin f \\ U_3 = F_3 - F_1 + mgd_J \sin\theta \\ U_4 = C_d\left(F_1 + F_3 - F_2 - F_4\right) \end{cases} \tag{12}$$

$F_i = C_t\Omega_i^2$ denotes the thrust force generated by motor i; Ω_i represents the speed of motor i; C_t and C_d are the thrust and drag coefficients, respectively; d_J is the distance between the vehicle's center of gravity (CG) and the center of the sphere joint (CSJ).

4.2. Quadcopter Control

To evaluate the GTB's performance, a 6-DOF flight controller (including attitude and position controller) is designed based on the quadcopter dynamics model [23-26]. The attitude controller consists of two loops, i.e., outer loop and inner loop (see Figure 7). The outer loop is a P-controller which calculates the angular rate setpoints. The inner loop is a PID-controller fed by the setpoints from the outer loop. The inner loop generates control signals that are allocated to be PWM signals before being sent to the motor's ESCs.

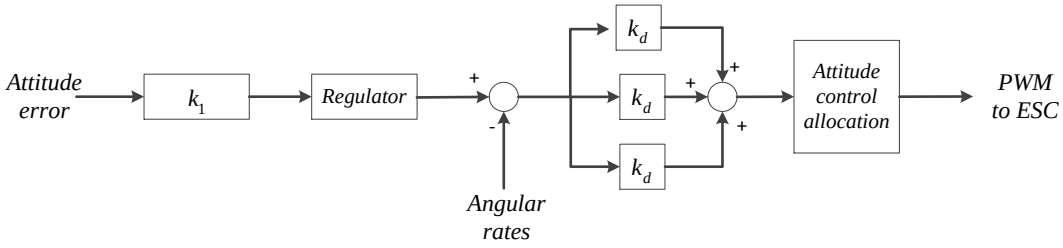

Figure 7: Attitude controller block diagram

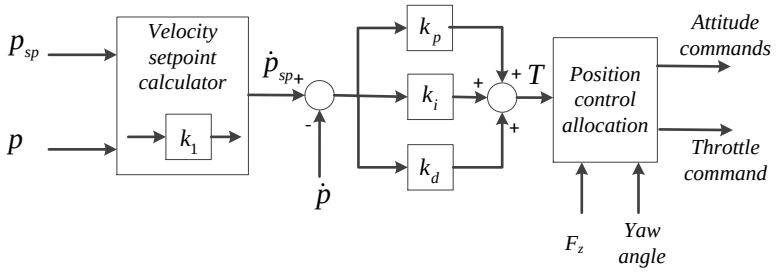

Figure 8: Position controller block diagram

The position controller (Figure 8) consists of a velocity setpoint calculator block that checks the distance, d, between the current position p and the destination p_{sp}, before calculating the corresponding velocity setpoint $\dot{p}_{sp}$. If d is smaller than a specified leash length, l_d, then the velocity setpoint is obtained as follows:

$$\dot{p}_{sp} = k_1(p_{sp} - p) \tag{13}$$

If d is larger than l_d, define v_{max} as:

$$v_{\max} = \sqrt{2a_{\max}\left(d - \frac{l_d}{2}\right)} \tag{14}$$

where, a_{max} is the desired maximum acceleration of the vehicle. Then, the velocity setpoints are calculated as:

$$\dot{p}_{sp} = v_{\max}(p_{sp} - p)/d \tag{15}$$

Remark 1: The control laws in (13) and (15) make the vehicle's response to be smooth even the position setpoint is far from the current position.

5. Experimental Results

Figure 9 shows experimental setup of the proposed GTB. The system's numerical parameters used for the experiment are listed in Table 1. At the start of each flight test, the vehicle is held in balance by some brackets. After powering on, the sensors process a series of initial setup and calibration steps, while mGCS is getting ready for data transmission. Once all start-up procedures have completed, the vehicle is armed and operated under stabilized control mode (3-DOF attitude control). The stabilizing brackets are released and the vehicle is free. In stabilized control mode, the attitude command can be sent to the vehicle either from the RC transmitter or from mGCS.

Table 1: System parameters for experiments

Parameters	Value and unit	Description
m	1.80 kg	Total mass of the quadcopter
J_x	0.0121 kg.m^2	Moment of inertia along x-axis
J_y	0.0119 kg.m^2	Moment of inertia along y-axis
J_z	0.0223 kg.m^2	Moment of inertia along z-axis
l	0.23 m	Arm length of quadcopter
d_J	0.11 m	Distance between the CG and CSJ
g	9.81 m/s^2	Gravitational acceleration
χ_x	0.25	Drag coefficient along x-axis
χ_y	0.24	Drag coefficient along y-axis
χ_z	0.31	Drag coefficient along z-axis
a_{max}	2.5 m/s^2	Maximum acceleration of quadcopter
$l_{d,xy}$	0.7 m	Leash length along x and y-axis
$l_{d,z}$	0.62	Leash length along z-axis

Once the attitude is stabilized, the control mode can be switched to position control mode (6-DOF), which means that the attitude controller will no longer receive any commands sent from the RC transmitter or the PC but directly from the position controller. Tables 2 lists the parameters of the attitude and position controllers. The position, velocity and acceleration of the vehicle were set to zero at the initialization. Afterward, they were simulated and updated automatically and can be reset to zero at any time during the test by using mGCS.

Table 2: Attitude and position controller's gains

Controller	k_1	k_p	k_i	k_d
Attitude				
roll	6.5	0.15	0.05	0.003
pitch	6.5	0.15	0.05	0.003
yaw	2.8	0.30	0.10	0
Position				
x, y	0.95	0.10	0.02	0.01
z	1.00	0.20	0.02	0

Figure 9: The proposed GTB

The experiment is conducted with several test cases, including: attitude stabilized flight, altitude flight, and position flight. In the following figures, the dashed line (if any) represents for the commanded value and the solid line represents the sensed value (or simulated value). Figure 10 shows the attitude and angular rate responses of the vehicle corresponding to an attitude step setpoint. It is seen that the vehicle tracks the setpoint with a small overshoot in the response which can be handled by tuning the attitude controller's gains.

Figure 11 presents the height, vertical velocity, throttle, and thrust force (less gravity) responses under an altitude step command. These results not only demonstrate the reliability of both the thrust force measurements and the PPA but also indicate the altitude controller was designed in a good manner.

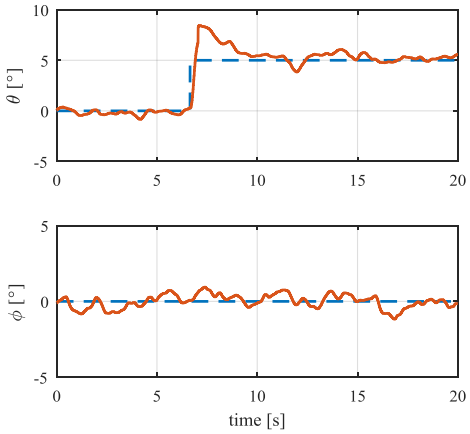

a) Attitude

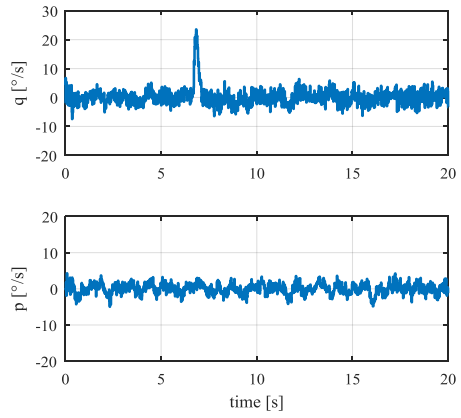

b) Angular rate

Figure 10: Results of an attitude stabilized flight

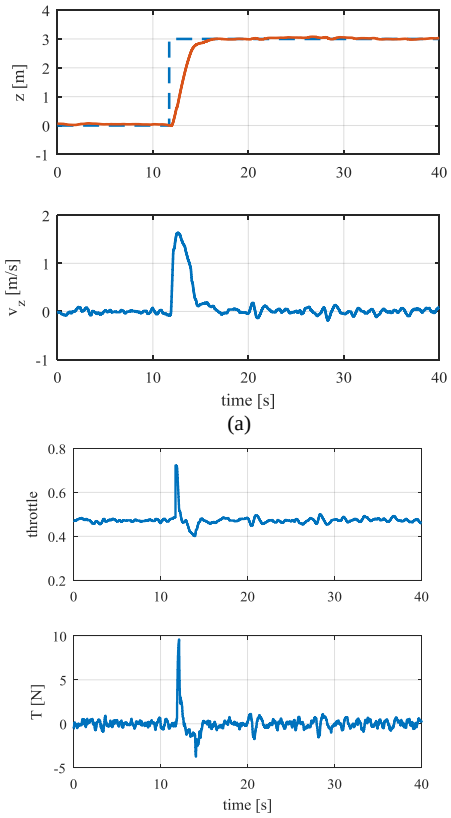

Figure 11: Results of an altitude flight

Figures 12 and 13 show the responses of the vehicle in a position hold (position setpoint is (0, 0, 2) meter) and a position waypoint flight, respectively. The stability and capability of the proposed system are proved through these results. These 6-DOF flight's performances also indicate the controllers are well designed with reasonable chosen values for the controller gains. These GTB tests provide significant references that allow developers to design, re-design, and fine-tune both the attitude and position controller without danger or crashing the vehicle.

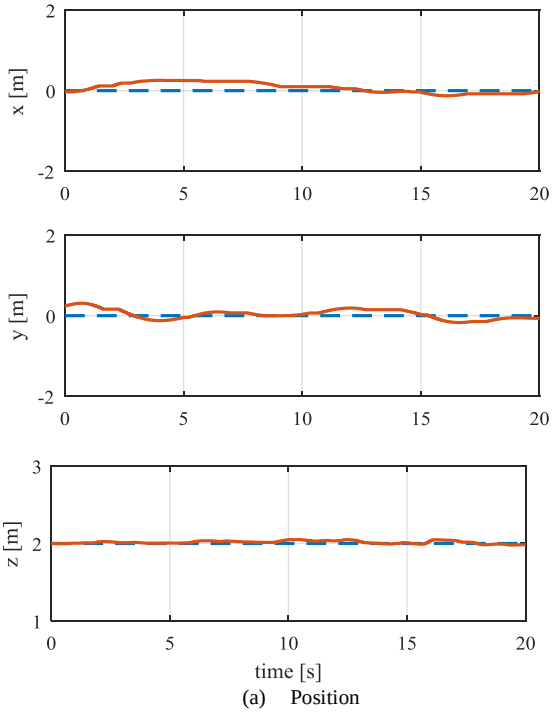

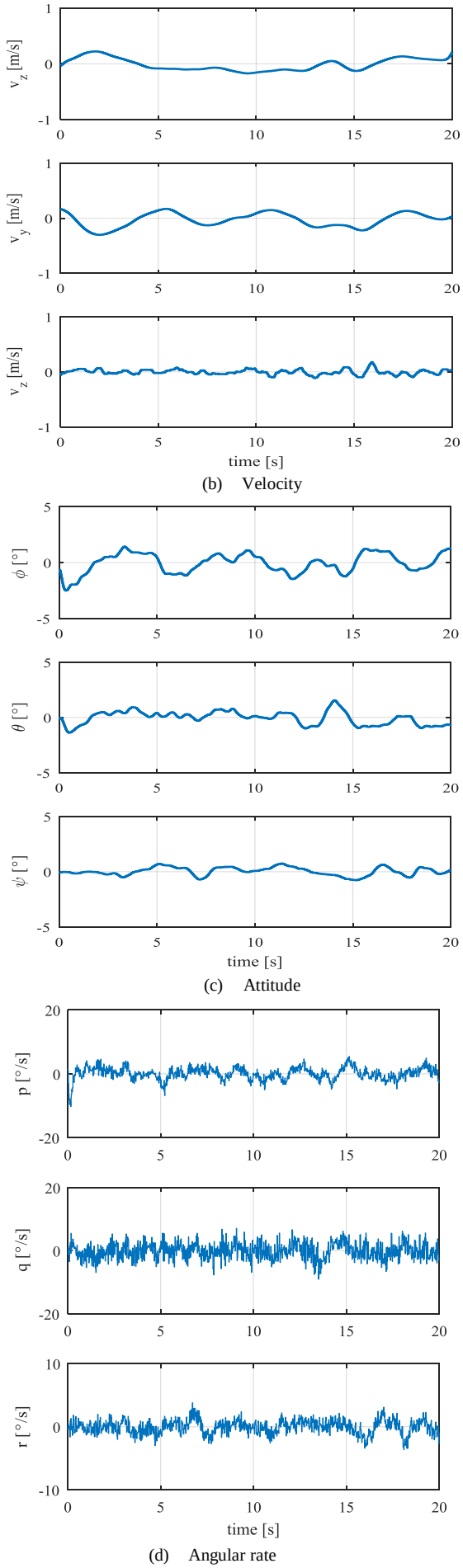

Figure 12: Results of a position hold flight

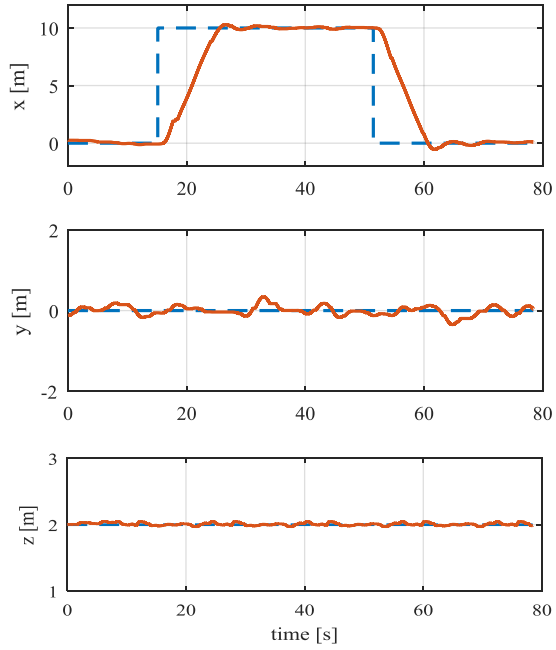

(a) Position

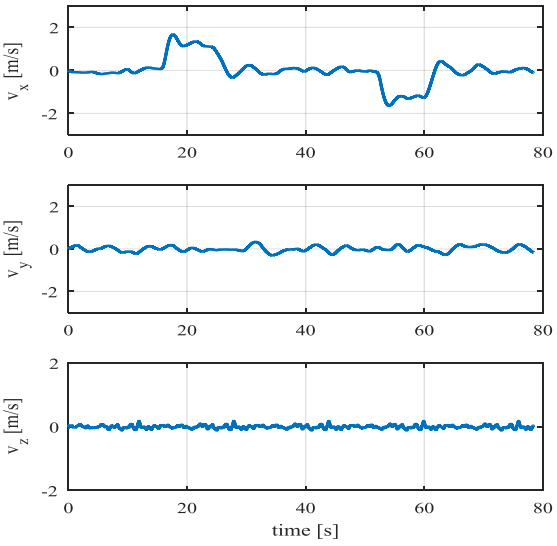

(b) Velocity

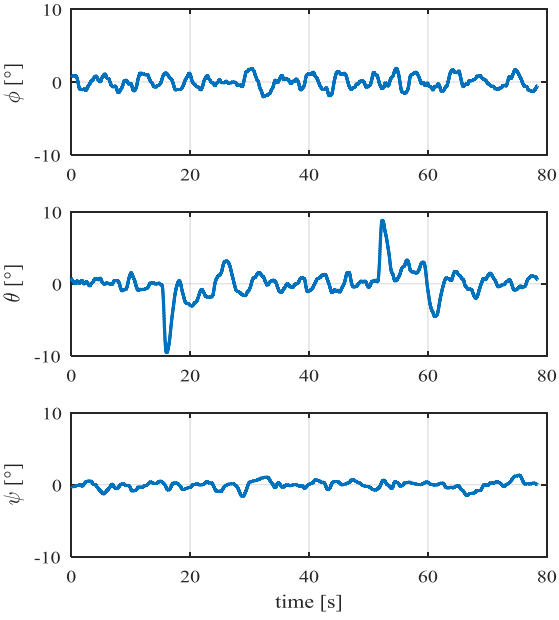

(c) Attitude

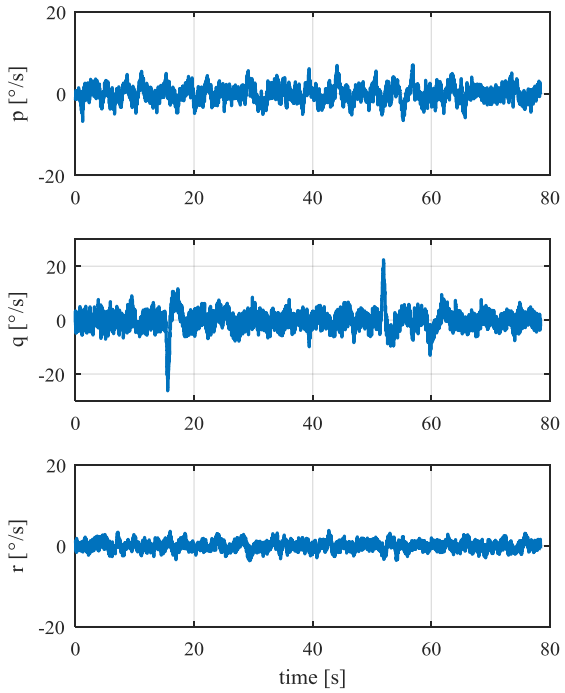

(d) Angular rate

Figure 13: Results of a position waypoint flight

While the experimental results underlined the value of the proposed GTB, the system still has noticeable shortcomings: The mass and friction of the sphere joint have neglected which introduces a discrepancy between performances of the on-GTB and actual outdoor flying behavior. The sensor noise and bias are variable when the vehicle is in motion. Although an LPF is applied to reduce the measurement noise, the variable bias cannot be removed entirely.

6. Conclusions

This paper proposes a 6-DOF multicopters ground testbed for the evaluation of attitude and position controllers. The experimental results demonstrate the feasibility and reliability of the proposed GTB. The system works successfully with attitude stabilized flight, altitude flight, and position flight. The GTB can accelerate multicopter development procedures provide a basis for a safe, reliable, and economic hardware-in-the-loop systems. Future work will employ a fusion algorithm to combine force data along the *x* and *y* axis and the IMU data with the aim to further improve PPA.

Acknowledgement

This work was supported by the Korea Institute for Advancement of Technology (KIAT) grant funded by the Korean government (Motie: Ministry of Trade, Industry & Energy) (No. N0002431).

References

[1] Frank Hoffmann, Niklas Goddemeier, Torsten Bertram. Attitude estimation and control of a quadcopter. International Conference on Intelligent Robots and Systems (2010): 1072-1077.

[2] Yushu Yu, Xilun Ding. A Quadrotor Test Bench for Six Degree of Freedom Flight. J Intell Robot Syst (2012) 68:323–338.

[3] Sepehr P. Khaligh, Alejandro Martinez, Farbod Fahimi, Chales Robert Koch. A HIL testbed for initial controller gain tuning of a small unmanned helicopter. J Intell Robot Syst (2014) 73:289–308.

[4] Yi-Rui Tang, Yangmin Li. Development of a laboratory HILS testbed system for small UAV helicopter. China. 2011.

[5] Kozuo Tanaka, Hiroshi Ohtake, Hua O. Wang. A practical approach to stabilization of a 3-DOF RC Helicopter. IEEE

Transactions on Control Systems Technology, vol. 12, no. 2, pp. 315-325, March 2004.
[6] J. G. B. F. Filho, C. E. T. Dórea, W. M. Bessa and J. L. C. B. Farias. Modeling, Test Benches and Identification of a Quadcopter. 2016 XIII Latin American Robotics Symposium and IV Brazilian Robotics Symposium (LARS/SBR), Recife, 2016, pp. 49-54.
[7] Scott D. Hanford, Lyle N. Long, Joseph F. Horn. A Small Semi-Autonomous Rotary-Wing Unmanned Air Vehicle (UAV). American Institute of Aeronautics and Astronautics.3. 2005-7077.
[8] Corentin Cheron, Aaron Dennis, Vardan Semerjyan, YangQuan Chen. A multifunctional HIL testbed for multirotor VTOL UAV actuator. Proceedings of 2010 IEEE/ASME International Conference on Mechatronic and Embedded Systems and Applications, Qingdao, ShanDong, 2010, pp. 44-48.
[9] Nikos I. Vitzilaios, Nikos C. Tsourveloudis. An experimental test bed for small unmanned Helicopters. J Intell Robot Syst (2009) 54:769–794.
[10] Huang Ran. Design and Demonstration of a Two-Dimentional Test Bed for UAV Controller Evaluation. All Theses.1874. 2014.
[11] Daniel Simon. Hardware-in-the-loop test-bed of an Unmanned Aerial Vehicle using Orccad.6th National Conference on Control Architectures of Robots, May 2011, Grenoble, France.14p., 2011.
[12] Bhargava, Abhishek. Development of a Quadrotor Testbed for Control and Sensor Development. All Theses. Paper 522. 2008.
[13] ROS.org. http://wiki.ros.org/. 2018.
[14] Dronecode. https://dev.px4.io/en/ros/. 2018.
[15] G. Cai. Unmanned Rotorcraft Systems. Springer - Verlag London Limited. 2011.
[16] Beard, Randal. UAV Coordinate Frames and Rigid Body Dynamics. Theory and Practice, Princeton University Press, 2012, ISBN: 978-06-911-4921-9.
[17] V. Kumar and N. Michael, "Opportunities and challenges with autonomous micro aerial vehicles," in Proc. 15th Int. Symp. Robotics Research, Flagstaff, AZ, Aug. 28–Sept. 1, 2011, pp. 1–16.
[18] M. Hehn and R. D. Andrea, "Quadrotor trajectory generation and control," in Proc. IFAC World Congress, Milano, Italy, Aug. 28–Sept. 2, 2011, pp. 1485–1491.
[19] Robert C. Leishman, John Macdonald, Randal W. Beard, Timothy W. McLain. Quadrotors and Accelerometers: State Estimation with an Improved Dynamic Model. IEEE Control Systems, vol. 34, no. 1, pp. 28-41, Feb. 2014.
[20] Philippe Martin and Erwan Salaun. The True Role of Accelerometer Feedback in Quadrotor Control.2010 IEEE International Conference on Robotics and Automation, Anchorage, AK, 2010, pp. 1623-1629.
[21] Rafik Mebarki, Jonathan Cacace, Vincenzo Lippiello. Velocity estimation using visual and IMU in GPS-denied environment.2013 IEEE International Symposium on Safety, Security, and Rescue Robotics (SSRR), Linkoping, 2013, pp. 1-6.
[22] Du Ho, Jonas Linder, Gustaf Hendeby, Martin Enqvist. Mass estimation of a quadcopter using IMU data.2017 International Conference on Unmanned Aircraft Systems (ICUAS), Miami, FL, USA, 2017, pp. 1260-1266.
[23] L. R. García Carrillo, A.E. Dzul López, Rogelio Lozano, Claude Pégard. Quad Rotorcraft Control. Springer - Verlag London 2013, pp. 23-34.
[24] W. Dong, G.-Y. Gu, X. Zhu, and H. Ding. Modeling and control of a quadrotor UAV with aerodynamic concepts. Int. J. Mech. Aeros. Ind. Mechatronic Manuf. Eng., vol. 7, no. 5, p. 437, 2013.
[25] J.-J. Xiong and E.-H.Zheng. Position and attitude tracking control for a quadrotor UAV. ISA Trans., vol. 53, pp. 725–731, May 2014.
[26] Gabriel M. Hoffmann, Haomiao Huang, Steven L. Waslander, Claire J. Tomlin. Precision flight control for a multi-vehicle quadrotor helicopter testbed. Control Engineering Practice 19.1023–1036. 2011.